



1 **Do sun spots influence the onset of ENSO and PDO events in the Pacific Ocean?**

2

3 *Franklin Isaac Ormaza-González¹, and María Esther Espinoza-Celi¹*

4 1) ESPOL Polytechnic University, Escuela Superior Politécnica del Litoral, ESPOL, (Facultad de
5 Ingeniería Marítima, Ciencias Biológicas, Oceánicas y Recursos Naturales), Campus Gustavo
6 Galindo Km. 30.5 Vía Perimetral, P.O. Box 09-01-5863, Guayaquil, Ecuador

7 Corresponding author: formaza@espol.edu.ec.

8 The sea surface temperature (SST), anomalies (SST), ONI (Oceanographic El Niño Index) and MEI
9 (Multivariate ENSO Index) in regions El Niño 1+2 (80°W-90°W, 0°-10°S) and 3.4 (5°N-5°S, 170°W-
10 120°W) as well as the Pacific Decadal Oscillation (PDO) and Atlantic Multidecadal Oscillation (AMO)
11 indexes were correlated to sun spots number (SS) from cycles (SS#) 19 to 24 (1954-2017). Degree-six
12 polynomial regression functions represented each of the six cycles with an average $r^2 > 0.89$
13 ($p < 0.001$). The series of correlations at different lag times (0, 6, 12, 24, 36 and 48 months) gave a
14 response time: 12-36 months. In the 1954-2017 period, the whole series of SS cycles did not show a
15 strong correlation with the variables and SST Anomaly in the El Niño areas 1+2 and 3.4. The highest
16 correlations r^2 were up to: 0.043, 0.029, 0.040 and 0.021 for PDO, MEI, ONI and SST Anomaly (in 3.4)
17 respectively, suggesting that there is still a correlation with high confidence ($p \leq 0.01$). Analysing for
18 the period 1990-2016, the correlations improved up to 0.11, 0.12, and 0.17 for ONI, SST (in 3.4) and
19 PDO correspondingly. The SST correlations against individual SS cycles in regions 3.4 and 1+2 were
20 up to 0.219 (SS# 23) and < 0.0675 (SS# 19) correspondingly. SST Anomaly, ONI and MEI correlated
21 with r^2 of 0.250, 0.3943 and 0.2510, one-to-one; the lag time was 24-48 months and linear curves
22 had positive slope. In general, in 1+2 there was found a more inconstant and lower correlation than
23 in 3.4 (where also MEI and ONI are measured). On the longer time scales, the PDO (alike AMO)
24 seemed to respond in 36-48 months to SS cycles showing a high degree of correlation coefficient r^2
25 of 0.625 (SS# 19) and 0.766 (SS# 24); whilst AMO index gave up to 0.490 (SS# 20) with similar lag
26 time. Cycles 19 and 24 showed a better correlation in general. During the ascending phases of each
27 cycle the SST in region 1+2 rendered correlation coefficient r^2 and p-value from 0.205 and 0.0008
28 (SS# 23) to 0.163 and ≤ 0.0044 (SS# 19). In the region 3.4, r^2 were from 0.870 (SS# 24), to 0.556 (SS#
29 23). In each SS cycle lag time was around 36 months; all of them occurred at the ascending phase,
30 except in cycles 20 and 24. SST anomaly registered r^2 from 0.662 to 0.254 in the ascending phase
31 with a response time 0-48 months and positive linear regression slope (except SS# 23). On the other
32 hand, the descending phase showed a predominantly lower r^2 : < 0.14 ($p < 0.01$). The region 3.4 had
33 better r^2 than in 1+2, from 0.897 (SS# 24) to 0.239 (SS# 21) respectively in the ascending phase
34 except cycles 20 and 24. The lag time was consistent at 36 months. The highest r^2 of 0.897 at the end
35 of the SS# 24 peak, coincided with one of the strongest El Niño (2014-2015) and the second highest
36 r^2 (SS# 22 ascending phase) with two consecutive strong El Niño 1991-1995. ONI and MEI also
37 showed strong correlation; the three highest r^2 matched dates of strong El Niño 1987-1989, 1955-
38 1957 and 1997-1998 in the ascending phase. During the descending phases, the correlation
39 coefficients were lower, and ranged from 0.6082 to 0.2938; but with a lag time 0-12 months, and
40 positive slope. The index MEI, as with ONI, registered r^2 lower during descending phases. The PDOs
41 were linearly correlated from 0.7677 to 0.2855 (12 to 24 months) and 0.3522 during ascending and
42 descending phases respectively. On the other hand, r^2 for AMO was up to 0.700. The strength of the
43 linear correlations substantially increased when the ascending and descending phase of each cycle
44 was analysed. During the ascending phase there is a stronger correlation than in the descending
45 phase. These results would indicate that warm events tend to occur in the ascending phase or at the
46 top of the cycle and have a delay time of around 36 months, whilst cold events are associated to a



47 descending phase but with a quicker response time. The sun spot activity should be considered as a
48 factor that could condition and trigger low (PDO and AMO) and high (ONI-El Niño) frequency
49 oceanographic events in the Pacific and Atlantic Oceans. During 2019, the cycle 25 should start, then
50 according to this work probably the next El Niño event would be around 2020-2021 or later.

51

52 **Key words:** Sun spots cycles, SST, SSTA, ONI, MEI, PDO, AMO, El Niño, La Niña

53

54

55

56 **Introduction.**

57 Essentially, the only external source of energy to Earth is the sun which constantly radiates a flux of
58 energy at a rate of 1360 W m^{-2} or $1.36 \text{ kJ m}^{-2} \text{ s}^{-1}$ (Monteith, 1972) or 1.92 ly day^{-1} (Ormaza-González
59 and Sanchez, 1983) to the upper external atmosphere of Earth; also called the solar constant.
60 Recently, Kopp and Lean (2011) have reported that the most accurate accepted solar constant value
61 of $1360.8 \pm 0.5 \text{ W m}^{-2}$ is lower than the canonical digit of $1365.4 \pm 1.3 \text{ W m}^{-2}$, which was established
62 in 1990. Of this flux of energy, 75-50 % reaches Earth and sea surface (Ormaza-González and
63 Sanchez, 1983; Lindsey, 2009) after it is reflected and/or absorbed by clouds, particles, gases, etc.
64 (Horning et al., 2003). 90-93% of that surface reaching energy is accumulated by the oceans
65 (Trenberth et al., 2014; Clutz, 2017). The solar constant is affected by the variable sunspot number
66 (SS, among other solar activity parameters) at around 0.1%, i.e. 1.361 W m^{-2} or 1.365 W m^{-2} . The
67 Hale cycle (around 11 years) is characterized by the increasing and then decreasing SS number
68 (Hathaway, 2015). Froelich (2013) suggested that the solar constant can vary up to 4.0 W m^{-2} in two
69 sun SS cycles, i.e. 22-year cycle, and proposed a simple relationship between SS and solar constant
70 (SC), by assuming a direct relationship between SC and SS

$$71 \quad SC = 1353.6 + 0.089 (SS) \quad (r^2 \text{ of } 0.71, 95\text{-}99\% \text{ confidence}).$$

72

73 The oceans store heat, alternately releasing and absorbing such energy. This system is basically
74 placed at the surface-subsurface of the oceans that interacts with the lower atmosphere. One
75 extensive work of Zhou and Tung (2010) reported the impact of SC on global SST along 150 years,
76 finding signals of cooling and warming SSTs at the valley and peak of the SS cycles; although
77 Schlesinger and Ramankutty (1994) did not imply an external force such as the SS, they reported a
78 global cycle of 65-70 years that is possibly affected by greenhouse anthropogenic gases, sulphate
79 aerosols and/or El Niño events. There are well known processes that are roughly periodic with low
80 (25-30 years) or high (3-5 years) frequency events such as the Pacific Decadal Oscillation (PDO,
81 Mantua et al., 1997; Mantua and Hare, 2002; Zhang et al., 1997; Yim et al., 2013), Atlantic



82 Multidecadal Oscillation (AMO, Enfield et al., 2001; Condrón et al., 2005; Gray et al., 2010) and
83 Interdecadal Pacific Oscillation (IPO, Henley et al., 2015); and El Niño (Busalacchi et al., 1983,
84 see **COAPS Library's**: <http://www.coaps.fsu.edu/lib/biblio/coaps-a.html>) or La Niña (Yuan and
85 Yan, 2012), respectively. During El Niño events, the surface and subsurface lose energy to the
86 atmosphere and the opposite during La Niña (Trenberth et al. 2014, Fasullo and Nerem, 2016) with
87 annual and interannual periods, while the decadal processes may take 25-30 years. The Interdecadal
88 oscillations have a series of impacts; e.g., the PDO gives rise to teleconnections between the tropic
89 and midlatitudes (Yoon and Yeh, 2010), and affects: 1) the ocean heat content (Wang et al., 2017), 2)
90 the lower and higher levels of trophic chain and small pelagic fisheries like tuna and sardines
91 (Ormaza et al., 2016a, 2016b), 3) biogeochemical air-sea CO₂ fluxes (McKinley et al., 2006), 4) the
92 frequency of la Niña/El Niño (Newman et al. 2003), etc. The interactions between decadal
93 oscillations PDO/IPO and AMO may affect also the ocean heat content (Chen and Tung, 2014). All
94 these low and high frequency oceanographic events have a direct impact on local, regional and
95 global climate patterns; there is some evidence that the driving source of energy is the sun (Grey et
96 al., 2010). Thus, Huo and Xiao (2016) have found positive strong correlation between El Niño 2015-
97 2016 and SS; afterwards, they also found a strong correlation between the latter and El Niño Modoki
98 index (Huo and Xiao, 2016). White et al., (1997) reported that heat anomalies produced by variable
99 solar irradiance are stored in the upper layer driving SST changes of 0.01-0.03 K and 0.02-0.05 K on
100 decadal and interdecadal periods respectively; also later Zong et al. (2014), in their review about the
101 impact of SS 11-year cycle and the multidecadal climate projections, have found global SST
102 variations of 0.08 ± 0.06 K and 0.14 ± 0.02 during the 11 and 22 years Hale Cycle, and that there is a
103 response lag of 1-2 years in relation to the SS (see also, Kristoufek, 2017). Liu et al. (2015) have
104 reported that apart from volcanic eruptions, effective solar radiation plays a role in the modulation
105 of decadal ENSO-like oscillation. More recently, Yamakawa et al. (2016) have reported that solar
106 activities in terms of SS numbers not only affect troposphere but also the sea surface.
107 Acknowledging that the SS is only a partial parameter to measure solar activity (Scafetta, 2014), this



108 work attempts to understand how the sunspots could affect low and high frequency oceanic events
109 such as the Pacific Interdecadal (PDO), the Atlantic multidecadal oscillation (AMO), Sea Surface
110 Temperatures, its anomalies and El Niño and La Niña events.

111

112 **Material and methods.**

113 Data for monthly **sun spot number** (SS) was taken from the Royal Observatory of Belgium, Brussels,
114 World Data Center SILSO (<http://www.sidc.be/silso/datafiles>). Data sources for other variables were
115 as follow: El Niño regions areas 3.4 (5°North-5°S, 170-120°W) and 1+2 (0-10°S, 90°W-80°W):

- 116 • **Sea surface temperatures (SST) and SST Anomaly:** The Monthly Extended Reconstructed
117 Sea Surface Temperature Version 4 (ERSSTv4, 1981-2010 base period). The Optimum
118 Interpolation 1/4 Degree Daily Sea Surface Temperature (OISST.v2, 1981-2010 base period),
119 <http://www.cpc.ncep.noaa.gov/data/indices/>.
- 120 • **Oceanic Niño Index (ONI)** (Huang et al., 2014): ERSST.v4 for El Niño/La Niña events since
121 1950 till December 2017:
122 http://www.cpc.ncep.noaa.gov/products/analysis_monitoring/ensostuff/ensoyears.shtml.
- 123 • **Multivariate ENSO index (MEI)** (Wolter and Timlin, 2011):
124 <https://www.esrl.noaa.gov/psd/enso/mei/table.html>.
- 125 • **Pacific Decadal Oscillation (PDO)**, based on Mantua Index): The PDO index is based on
126 NOAA's extended reconstruction of SSTs (ERSST Version 4). It is constructed by regressing
127 the ERSST Anomaly against the Mantua PDO index for their overlap period, to compute a
128 PDO regression map for the North Pacific ERSST Anomaly. The ERSST Anomaly are then
129 projected onto that map to compute the NCEI index. The PDO index closely follows the
130 Mantua PDO index at: <https://www.ncdc.noaa.gov/teleconnections/pdo/> (Wolter and Timlin
131 1993, 1998 and 2011).



132 • **Atlantic Multidecadal Oscillation** index:

133 <https://www.esrl.noaa.gov/psd/data/timeseries/AMO/>.

134 All indexes have data from April 1954 to December 2017. The analysis was done using Excel
135 and/or R statistical tools. The correlation exercises were executed using SS solar cycles as
136 complete time series against SST Anomaly (in 3.4 and 1+2), ONI, MEI, AMO and PDO indexes.
137 Correlations with lags of 0 to 48 months were carried out. For the SS cycles 19-23 and their
138 impact on the above mentioned dependent variables, correlations were carried out for the
139 whole time series 1954-2017, for 1990-2016, for each cycle and for their respective ascending
140 and descending phases. Spectral analysis and polynomial regression fitting curves were
141 determined to obtain the slope of the ascending phases; the slopes were correlated to the
142 oceanographic indexes.



143 **Results and discussion:**

144

145 The time series (1954 to 2016) of SS, PDO, AMO, ONI and MEI are shown in Fig. 1. PDO, AMO, ONI
146 and MEI start at time: 0, 12, 24 and 36 months (panels a, b, c and d respectively); whilst SS series
147 starts at t=0 in the four panels. It has been reported the lag time responses to SS cycles of some
148 indexes are around 12-36 months (e.g., Zhao et al., 2014). From 1954 to the present, there has
149 occurred the cycles 19 to 24; cycles have a period of around 11 years (Hathaway, 2015); Dicke (1978)
150 established 11.2 years. The highest peak is seen in cycle 19 with around 250 SS/month; then, the
151 next cycle goes down to <150, but the peak of cycle 21 jumps to around 200, to decrease steadily
152 from cycle 22 to 24 to just over 100 SS/month. Cycle 24 is one with the lowest contemporary peaks
153 of a SS cycle comparable only to cycles 12-15 (around 1880-1930), and the lowest in the last 200
154 years (Clette et al., 2014). The negative or cold PDO phases (1947-1976, 2000-june/2016) are within
155 SS cycles 19 -20 and 23-24, but cycles 21 and 22 are within the positive or warm phase of the PDO
156 (1977-1999). As PDO and AMO indexes are displaced from 0 to 36 months on the time scale, some
157 peaks and troughs can be seen; these are at ascending and descending parts of the SS cycles; thus,
158 during cycles 19-20 and 23-24 PDO indexes are basically negative, and on the contrary during 21-22;
159 the exception is around 1990, where there is a strong negative peak. However, AMO phases seem to
160 be in opposition to and overlapping the SS cycles; a cold phase of AMO is between 60s and 90s,
161 whilst the warm one is from the 90s to the present (McCarthy and Haigh, 2015).

162

163 The ONI and MEI curves, both indicators of ENSO events, behave similarly throughout the study
164 period (April 1954 – December 2017). However, MEI has the highest anomaly peaks (> 2) compared
165 to ONI, specifically in: 1995, 1980 and mid-2016. In general, ONI and MEI curves indicate the highest
166 positive anomalies between 1978 and 1995, a period that coincides with the warm and cold phases
167 of PDO and AMO respectively. The opposite occurs before and after this period due to the inversion
168 of phases. In addition, the highest peaks of both indexes only occur during the ascending and



169 descending phases of the solar cycles; that is, they never coincide with the maximum period of
170 sunspots of the cycles. The two highest MEI peaks occur during the descending phase of solar cycle
171 21 and ascending phase of solar cycle 23. In the mid-2016 (cycle 24) both indexes increased
172 reaching the third highest peak of this period during the descending phase of the solar cycle 24. On
173 the other hand, negative peaks of these indexes are noted to occur either in the high or low plateau
174 of the SS curves.

175

176 The number (N) of data in the analysis were: 765 (1965-2017); 312 (1990-2016); 108 (1990-1999);
177 192 (2000-2016). For individual cycles 19 to 24: 127, 141, 124, 117, 141 and 120 respectively. In the
178 same order for ascending-descending phases: 48-80, 50-92, 43-82, 33-85, 51-51 and 74-47. The
179 degrees of freedom of residual were N-2. The degree of correlation in terms of Pearson coefficient is
180 referred as: High, moderate and low when its ± 0.5 and ± 1.0 , ± 0.3 to ± 0.49 and ± 0.29 respectively
181 (<http://www.statisticssolutions.com/pearsons-correlation-coefficient/>). All linear regression
182 residuals were autocorrelated using the Durbin-Watson (DW) test (Montgomery et al., 2001); for
183 1954-2017, 1990-2016, 1990-1999, 2000-2016, individual cycles, and ascending-descending phases.
184 The DW tests for the long time series averaged 0.122, for individual cycles varied from 0.10 to 0.63
185 with an average of 0.18, and for the ascending and descending phases averaged 0.40 and varied
186 from 0.1 to 2.24. SST Anomaly in region 1+2 has the lowest and PDO the highest.

187

188 **The whole series (1954-2017) correlations.** All variables (Table 1) were correlated in a linear and
189 polynomial (n= 2 to 6 order) basis using different lag times (0, 6, 12, 24 and 48 months) along the six
190 SS cycles. Polynomial correlation (not shown) as well as linear ones displayed poor correlation
191 coefficients; however, for the latter, the highest r^2 ($p \leq 0.01$) coefficients were found to occur at lag
192 time somewhere between 12 and 24 months, except for AMO (36-48 months). For SST and SST
193 Anomaly in 1+2 there was found no correlation. These results agree somewhat with Kristoufek



194 (2017), who suggested a surface thermal response of around 24-36 months. The highest correlation
195 r^2 values were up to: 0.043, 0.029, 0.040 and 0.021 for PDO, MEI, ONI and SST Anomaly (in 3.4)
196 respectively; suggests that there is still a correlation with high confidence (p -value ≤ 0.01), though of
197 small r^2 . This fact could be explained as the sun activity (sun spots) in the long run balances
198 throughout the ups and downs of the cycles. This exercise would suggest there is not a good
199 correlation on these indexes in the Pacific and Atlantic at the studied time scale; nonetheless, on
200 longer time series, where SS are affected by other sun internal processes; e.g., the alleged Minimum
201 of Maunder (Eddy, 1976, Shindell et al., 2001, Ineson et al., 2015, Mörner, 2015, etc.) can impact on
202 a global and regional basis. Recently, Lockwood (2010 and 2013) has reported that a grand solar
203 minimum is coming as the behavior of the SS cycle 24 is developing; i.e., it is being observed that for
204 the last 9300 years, there has not been such solar activity decline as found in cycle 23 to 24. This fact
205 gives a likely occurrence of a solar minimum that may last through cycles 24, 25 and 26 (Hady, 2013).
206 Under these circumstances, it was decided to analyze correlations using individual cycles, from the
207 19 to 24.

208

209 **Period 1990-2016.** Further analysis was carried out using the period 1990 to 2016, that includes
210 cycles 22, 23 and 24. The time series was also split in 1990-1999 and 2000-2016, because during
211 1990-1999: a strong (1991-1992), moderate (1994-1995) and the strongest El Niño (1997-1998) of
212 the XX century occurred. On the other hand, in 2000-2016 (cold phase PDO) also a strong a La Niña
213 (2000-2002 and 2010-2012) and El Niño Modoki in 2015 (Huo and Xiao, 2016) were registered. The
214 Figure 4 shows again a poor r^2 : < 0.011 ($p > 0.246$), for the SST Anomaly in region 1+2 (blue bars),
215 although this region was gravely affected by the strong El Niño 1997-1998 which brought hundreds
216 of casualties and billions of US dollar losses to the Ecuadorian infrastructure (Glantz, 2001). The
217 linear correlation r^2 of SST in 3.4 (red bars) was around 0.1193 ($p \leq 0.00001$) in the whole period,
218 whilst a bit higher in the period 1990-1999: 0.1519 ($p \leq 0.01$). The ONI (green bars) was up to 0.1436



219 ($p \leq 0.02$) correlated to SS in the period 1990-2000 where high positive SST Anomaly were present for
220 almost 6 years. ONI correlated better than SST Anomaly in 3.4. The Pacific Decadal Oscillation (Fig.
221 4., grey bars) had an r^2 of 0.276 ($p < 0.0001$), in the period 2000-2016 (PDO in a cold phase), with a
222 Pearson correlation of 0.523 that can be considered as high
223 (<https://www.statisticssolutions.com/pearsons-correlation-coefficient/>). However, for the period
224 1990-1999 it was 0.239 and for the whole period was 0.402; i.e., a poor and fair degree of
225 correlation respectively.

226

227 **Individual Cycles.** Correlation analysis was split into SS cycles, from 19 to 24. The SS and SST r^2
228 correlation coefficient indicated poor correlation and confidence ($p \geq 0.05$) in region 1+2 in all cycles
229 (Fig. 2); most of the correlation r^2 were < 0.050 , except in cycle 19, where a r^2 of 0.0675 ($p = 0.0032$);
230 in cycles 21 and 23 the highest r^2 was 0.046 ($p = 0.0173$) and 0.048 ($p = 0.037$) respectively. The lag
231 time varied between 6 to 36 months. In region 3.4 correlation were variable and rendering a r^2 up to
232 0.219 ($p \leq 0.0001$) and 0.213 ($p \leq 0.0001$) for cycles 23 and 19 respectively, with a lag time of 12-36
233 months with an exception in cycle 19 (Fig. 2), where the highest coefficient was after 6 months lag
234 time. Cycles 20 and 22 had r^2 of 0.105 ($p \leq 0.0001$) and 0.074 ($p = 0.003$) in the same order. The slopes
235 of the linear regression curves with the highest r^2 were positive in region 3.4, indicating a direct
236 correlation between SST and SS cycles. However, cycles 22 and 23 in the region 1+2 exhibited
237 inverse correlation (Fig. 2). Further polynomial correlation ($n = 2$ to 6) analysis did not render any
238 substantially better r^2 . In general, higher correlation was found in 3.4 than in 1+2.

239

240 **Anomalies SST.** SST Anomaly can change in terms of the reference used; there are 5 versions of ERRS
241 (Huang et al., 2017). These versions are nowadays used almost in every study related to El Niño;
242 currently is the version 5. In this work we used the ERRSv4 (Huang et al., 2014); Huang et al. (2017)
243 stated that there is not a noticeable difference between ERRSv4 and ERRSv5. The anomalies of SST in



244 3.4 and 1+2 were also correlated against every cycle; correlation r^2 was not found better than 0.396
245 ($p \leq 0.0001$) in both regions, with higher variability in 1+2 than 3.4 either in response time and
246 correlation coefficient (Fig. 3). In region 3.4, the highest correlations were 0.289 ($p \leq 0.0001$) and
247 0.270 ($p \leq 0.0001$) during cycles 19 and 23 respectively, with a lag time between 12 and 36 months,
248 and both during cold phases of PDO (1955-1978, and 2000-present). Surface winds plus other
249 oceanographic variables (e.g.; upwelling) could play an important role in this high variability; these
250 winds are not only generated in this area but farther away, even by the trade winds of the western
251 Atlantic (Ormaza-González and Cedeño, 2017). Also, ENSO processes in the western Pacific could add
252 variability in the SST Anomaly. The slopes of the linear correlation were basically positive for 3.4 and
253 negative for 1+2, similar as for SST correlations for cycles 19, 23 and 24 (cold PDO phase) for the
254 highest r^2 . Again, the anomalies in 3.4 were better correlated than in 1+2 region.

255

256 **ONI.** The El Niño index (Fig. 5) displayed r^2 values from around 0.053 ($p=0.01$, cycle 22) up to 0.25
257 ($p < 0.0001$, cycle 24), in a poor to fair correlation with a positive slope mainly in SS#: 19, 23 and 24.
258 During SS# 24, ONI reached high values of 2.6C (Nov-Dec-Jan 2015/2016) and -1.7C (Oct-Nov-Dec
259 2010). The highest r^2 were again found again somewhere 24-48 months lag time. Cycle 21 did not
260 show any confident correlation with ONI; however, cycles 20, 22 and 24 had r^2 of 0.144 ($p < 0.001$),
261 0.131 ($p < 0.0001$) and 0.252 ($p < 0.0001$) respectively, with lag times of: 48, 12, and 24 months
262 respectively. Recently, Huo and Xiao (2016) found strong correlation between SS and El Niño Modoki
263 during 2015 (SS# 24). The variability of the r^2 could arise from: 1) SS number importantly varying
264 from one month to another, 2) regional meteorological conditions (particularly cloudiness), ocean
265 surface currents that exchanges heat of the region 3.4, Kelvin waves (Gill, 1982), the Southern
266 Oscillation Index (SOI: Southern Oscillation Index: <http://www.cpc.ncep.noaa.gov/data/indices/soi>),
267 etc., that in turn affect the SSTs; and, on top of that, 3) the way ONI is obtained; i.e., ONI has variable
268 reference period of 30 years; thus for 1950 to 1955 the reference period is 1936-1965; for 1956-



269 1960; 1941-1970; the ERRSv4 uses the period 1981-2010. The reference period is moved every 5
270 years (Lindsey, 2013); the most recent ONIs (v4/v5) are supposed to have better and more
271 consistent data as equipment acquisitions improve in time.

272

273 **MEI.** This index, which is another index for El Niño events, correlated at lower r^2 ; thus, the highest
274 value was 0.3943 ($p < 0.00101$, SS# 19), the next 0.3028 ($p < 0.00001$, SS# 24), 0.2421 ($p < 0.00001$,
275 SS# 23) and 0.1566 ($p < 0.0001$, SS# 20); in cycles 21 and 22 there was not found correlation better
276 than 0.1232 ($p < 0.0001$). The lag time ranges from 24-48 months, and linear regression curves were
277 with mainly positive slope.

278

279 **PDO.** This interdecadal index (Fig. 5) is linearly correlated to SS cycles somewhere between 36 and
280 48 months lag time, with highest r^2 of 0.391 ($p < 0.00001$) in cycle 19, and 0.586 ($p < 0.00001$) for
281 cycle 24), with strong correlation: 0.625 and 0.762 respectively. Both cycles are within the cold
282 phase PDO. The next highest r^2 with p-values < 0.0001 were 0.218, 0.1361, 0.218 and 0.260 for
283 cycles 20-23. In all cycles, the highest r^2 were positively correlated, except cycle 20. For some
284 reason, there appears a better fit with both PDO and ONI in cycles 19 and 24, which are within the
285 period of cold phase of PDO, even though these cycles have remarkable different shape and peaks
286 (Fig. 12); cycle 19 registered SS counts over 250 whilst cycle 24 just around 100; also, the plateau of
287 their peak was different: very sharp and extended respectively.

288

289 **AMO.** This index proved to render correlation coefficients r^2 up to 0.490 ($p < 0.00001$) and down to
290 0.162 ($p = 0.0004$) in cycles 20 and 24 respectively) with a lag time of 48 months, which is the elapsed
291 time where the highest correlation was found in cycles 20, 23 and 24, whilst at cycle 19, 21 and 22
292 the elapsed time was 24-36 months. Gray et al. (2016) reported lag time response of mean-sea-level



293 pressure over the Atlantic to SS cycles of 36-48 months, in a longer time series study of 32 solar
294 cycles. The Fig. 6 shows the bar distribution of the r^2 ; it displays linear regression with positive and
295 negative slopes for cycles 19, 23 and 24; and 20 to 22, respectively. This coincides with the phases of
296 the AMO, negative from around 1965 to 1998 (SS# 20-22), and positive; 1930-1965 (SS# 19) and
297 after 1998-present (SS# 23-24), <http://appinsys.com/globalwarming/amo.htm> . It is noteworthy to
298 say that the slopes of the PDO and AMO linear regression show to be negative/positive respectively
299 in cycle 21 and 22, but in concordance in cycles 19, 20, 23 and 24 whose periods correspond to the
300 cold phase PDO.

301 **Ascending and descending phases** of solar cycles. As the SS cycles, which last about 11.2 years,
302 impact on variables studied on a response time from 24 to 36 months, there was the need to study
303 their influence during the ascending and descending phases, which have roughly 5-6 years duration.
304 Polynomial regression analysis was performed to establish a function that could best describe every
305 SS cycle. Sixth-order polynomial curves (Fig. 12) were found to render a very strong correlation
306 coefficient averaging 0.89 ($p \leq 0.001$). The functions allowed to analyse the correlations in the
307 ascending and descending phases.

308

309 **SST in 1+2 and 3.4.** In region 1+2, the highest correlation coefficient r^2 and p-value were 0.205 and
310 0.0008 (SS# 23), 0.189 and ≤ 0.0036 (SS# 21), and 0.163 and ≤ 0.0044 (SS# 19). All linear regression
311 coefficients r^2 over 0.0847 ($p < 0.05$ to $= 0.0008$) occurred in the ascending phase of the SS cycles, but
312 lower ones occurred in the descending phase, with no definite lag time pattern from 0 to 36 months.
313 The slope (positive/negative) of the linear regression (Fig. 7) curves showed no pattern. These low
314 and variable r^2 reflect that region 1+2 is subjected to the conjunction of many diurnal and seasonal
315 oceanographic and meteorological variables; for example, during the first quarter of 2017 (cycle 24),
316 in 1+2 there was higher than usual SST because the southern trade winds in eastern Pacific
317 weakened and the North Atlantic ones strengthened; thus, these passed through the Panama



318 Isthmus, and blew warm (up to 30C) surface waters from Panama Bay down south to 1+2 provoking
319 a rapid and relatively short lived surface warming (Ormaza-González and Cedeño, 2017), while
320 region 3.4 was registering La Niña conditions. This cold event also strengthens the Cromwell
321 Undercurrent (Knauss, 1959) and Humboldt (Montecino and Lange, 2009) currents related to
322 upwelling processes in 1+2. During the ascending phases of the cycles, the correlation of SSTs was
323 higher than in the descending phase of cycles. All these facts would mask the SS signal in this area.

324

325 In the region 3.4, the maximum r^2 of SST in each SS cycle was found at lag time of 36 months; all of
326 them occurred at the ascending phase, except in cycles 20 and 24. The four highest r^2 were 0.870
327 ($p=0.021$, 24), 0.613 ($p<<0.0001$, 22), 0.574 ($p<<0.0001$, 19), and 0.556 ($p<<0.0001$, 23); i.e., the
328 Pearson coefficients were: 0.9327, 0.7803, 0.7576 and 0.7456, respectively, which show strong
329 degree of linear correlation. Linear regression slopes were variable (Fig. 7), although there was a sort
330 of tendency in cycles 20, 21 and 22 (warm PDO) for negative slopes and for positive slopes for cycles
331 19, 23 and 24 (cold phase PDO). In 3.4 the SST response to SS was much clearer than 1+2, as in this
332 region (10N-10S and 120W-180W) there is not influence of coastal processes. The highest r^2 (0.870,
333 $p=0.021$; lag time 36 months) in the descending phase in cycle 24 coincided with the strongest El
334 Niño, and the second-highest r^2 (0.613, $p<<0.00001$) during ascending phase of cycle 22 with two
335 consecutive strong El Niño 1991-1995; the third r^2 (0.574, $p<<0.00001$) during cycle 19, with el Niño
336 1955-1957, and finally the fourth r^2 (0.556, $p<<0.00001$) with 1997-1998 warm event during cycle 23.
337 It seems that short time expressions of SS cycles, either on their initial ascending or descending
338 phases, trigger effects on the SSTs.

339

340 **SST Anomaly.** In region 1+2 (Fig. 8), the anomalies registered high r^2 ($p<<0.0001$) of 0.662 (SS# 22),
341 0.637 (SS# 19), 0.523 (SS# 21), 0.480 (SS# 23), 0.359 (SS# 24); and 0.254 ($p=0.0002$, SS# 20)
342 respectively, in the ascending phase of the SS cycles and with a positive linear regression slope



343 (except SS# 23). The response lag time was somewhere between 0 to 48 months. On the other hand,
344 the descending phase showed a predominantly lower r^2 , less than 0.14 with lower significance ($p \leq$
345 0.02), with the exception in SS# 19, 0.304 ($p < 0.0001$). The results indicate that during cold phase
346 PDOs, as the surface ocean waters in 1+2 are relatively colder, the correlations tend to be higher.

347

348 **SST Anomaly in 3.4.** There was a high and consistent r^2 (Fig. 8) that reached up to 0.897 ($p=0.014$;
349 SS# 24); 0.863 ($p < 0.0001$; SS# 22); 0.665 ($p < 0.0001$; SS# 19), 0.826 ($p < 0.0001$; SS# 23), then fell
350 to 0.211 ($p=0.008$; SS# 20); 0.239 ($p=0.0009$; SS# 21) respectively; all of them were in the ascending
351 phase except cycles 20 and 24. The lag time was consistent at 36 months. Linear regression slopes
352 were variable (Fig. 8); negative slopes in cycles 20-22 (warm phase PDO); and positive slopes in 19,
353 23 and 24 cycles (cold phase PDO). The highest r^2 of 0.897 in the initial moment of the descending
354 phase in 24 coincided with one of the strongest El Niño and the second r^2 (SS# 22 ascending phase)
355 with two consecutive strong El Niño 1991-1995. The third and fourth highest r^2 were during El Niño
356 1955-1957 and 1997-1998 warm event (SS# 23 ascending) respectively. The results are suggesting
357 that SS cycles are strongly correlated to SST Anomaly in both El Niño regions, but much more in 3.4.

358

359 **The ONI index.** This index as well as SST and its anomalies in 3.4, were equally strongly associated
360 with the ascending phase of the SS cycles (Fig. 9); with a lag time of 24-36 months and the highest
361 correlation r^2 per each cycle were in the ascending phase; the predominant linear regression curve
362 slopes were positive, except SS# 20. The highest r^2 ($p < 0.0001$) were: 0.817 (SS# 22), 0.693 (SS# 19),
363 0.637 (SS# 23), 0.3547 (SS# 24), 0.2876 (SS# 20); 0.1936 ($p=0.003$, SS# 21). The three highest r^2
364 match with the dates of strong El Niño 55-57, 87-89, and 97-98 (Fig. 9) with positive slope and
365 ascending phase. The ascending phase coincides with El Niño, or after 2-3 years the peak or valley of
366 the cycle. In the descending phase the r^2 ($p < 0.0001$) in cycles 24, 23, 22 and 20 with 0.366, 0.284,



367 0.255, and 0.242 respectively. All of them have a lag time 0-12 months and positive slope. Cycles 19
368 and 21 showed neither strong correlation (<0.1) nor confidence ($p=0.2$).

369

370 Warm events tend to occur in both ascending/descending phase after the peak/trough, and have a
371 delay time of 36 months, which is like what was found by Huo and Xiao (2016). The descending
372 phase of the cycles (Fig. 9), with a smaller slope than the ascending phase, produce quicker
373 responses (0-12 months) of the ocean surface SST and ONI that could trigger neutral or cold events
374 more cogently; most of la Niña events occur during the descending phase or approaching the cycle
375 minimum (Fig. 10). The weakest SS# 24 has had three La Niña: 2007-2009, 2010-2012, 2016-2017
376 (Fig. 12). A plausible reason is that during this cycle the number of sun spots (i.e., sun activity) is the
377 lowest in the last two centennials (Clette et al., 2014); therefore, less energy has hit the ocean
378 surface producing a cooling effect. Two important exceptions are La Niña 1988-1989 (22) and 2000-
379 2002 (cycle 23) that occurred in the ascending phase.

380

381 **The MEI index.** The Multivariate ENSO Index does not only consider the SST Anomaly but also sea-
382 level pressure (Allan and Ansell, 2006) and other variables. These variables include surface winds
383 (meridional and zonal), surface air temperature and total cloudiness fraction of the sky (Wolter and
384 Timlin, 1998). The MEI correlated at slightly lower levels with SS cycles with r^2 : 0.784 ($p \leq 0.0001$),
385 0.770 ($p < 0.0001$), 0.5972 ($p \leq 0.0001$); 0.3396 ($p \leq 0.0001$); 0.2368 ($p=0.0003$); and 0.222 ($p=0.001$)
386 for SS cycles 19, 22, 23, 24, 20, and 21, respectively. All of them in the ascending phase of the cycles
387 with a lag time from 12 to 48 months (except cycles 23 and 24), with a positive linear regression
388 slope; except 22 and 20 where the r^2 was largest with zero lag. During the descending phase, like the
389 ONI, the r^2 were lower: 0.321 ($p=0.0004$, SS# 24); 0.3145 ($p < 0.0001$, SS# 19); 0.2234 ($p < 0.0001$,
390 SS# 22); 0.2088 ($p < 0.0001$, SS# 20), and 0.1438 ($p=0.0002$, SS# 23) with positive slope (except 20)
391 and lag time, predominantly 0-48 months; cycle 21 did not have a r^2 above 0.010 ($p > 0.02$). For the



392 index MEI, as with ONI, the r^2 were much lower during descending phases. The descending phases
393 showed to be also associated with la Niña, thus resembling somehow what was found with ONI. The
394 lower correlations could be because MEI has more influencing factors than ONI, which could obscure
395 the signal from the sun irradiation.

396

397 **PDO.** The Pacific Decadal oscillation linear correlation with SS gave larger r^2 in most of cycles except
398 in cycle 20 (0.2589; $p \leq 0.0002$) and 21 (0.2855; $p=0.0002$); thus 0.7677 ($p \leq 10^{-12}$), 06577 ($p \leq 10^{-12}$),
399 0.6734 ($p \leq 10^{-7}$) and 0.5062 ($p \leq 10^{-7}$) for the ascending phase SS# 19 (Apr/54-Nov/58), SS# 24
400 (Jan/08-Feb/14), SS# 22 (Sep/86-Jan/89) and SS# 23 (May/90-Jun/00) respectively. All these
401 coefficients were obtained at a lag time of 12-48 months, except 22 and 23 ($t=0$). The slopes of the
402 linear regressions were mainly positive during cold phase PDOs (cycles 19, 23 and 24), except cycle
403 20 when a cold PDO was transitioning to a warm PDO (21 and 22). The figure 10 shows that linear
404 correlations in cycles 19, 21, 23 and 24 showed positive slopes. The two highest r^2 are at lag time of
405 12-36 months, for cycles 19 and 24, as have been reported in other works (e.g., Huo and Xiao, 2017).
406 During the descending phase, the correlation r^2 tended to be much lower, with the highest 0.3522
407 ($p < 0.00001$) and 0.3452 ($p < 0.00001$) at cycles 19 and 20. Sun spot energy variations on long time
408 scale (van Loon et al. 2007), even at very weak changes, could produce decadal and millennial
409 timescale impacts on global circulation thermohaline that affect in turn heat distribution (Bond et al.
410 2001, Gray et al., 2013).

411

412 **AMO.** The Atlantic Multidecadal Oscillation index is in opposite phase to the PDO (Enfield et al.,
413 2001; Condrón et al., 2005); i.e., warm: 1930-1964 and 2000-present (cold PDO), and cold: 1965-
414 1999 (warm PDO). The correlations were generally higher at the descending phase of the SS cycles
415 (Fig. 11), practically the opposite to those for SS vs PDO, ONI, MEI, SST Anomaly. However, the
416 highest r^2 occurred on ascending (A) and descending (D) phases of SS cycles, thus: 0.700 ($p < 10^{-10}$),



417 0.558 ($p < 10^{-10}$), 0.468 ($p < 10^{-10}$), 0.434 ($p = 0.03$), 0.411 ($p < 0.00001$) and 0.191 ($p = 0.001$) for
418 cycles 20A, 22D, 19D, 24D, 21A and 23A, one-to-one. These r^2 showed strong degree of correlation,
419 although lower comparing to PDO. The lag time was basically between 24-48 months.



420 **Discussion and Conclusions**

421

422 **Period 1954-2017.** The SS peaks of the studied cycles decreased smoothly (Fig. 10); the SS peak
423 counts were around: 225 (SS# 21), 210 (SS# 22), 180 (SS# 23), and 110 (SS# 24), whilst at the
424 minimum for the cycles, SS counts were around 20-25. Thus, it could be said that Earth is receiving
425 less solar energy over these almost 7 decades. The reduction of SS peaks has been associated with
426 the beginning of Maunder Minimum (Mörner, 2015). Ineson et al. (2014) are projecting lower peaks
427 for next SS cycle (SS# 25); in fact, presently the SS counts per month are as low as 1.6 (July 2018) and
428 average 8.5 (Jan-Aug 2018) (<http://www.sws.bom.gov.au/Solar/1/6>), with expected counts to
429 decrease to 5.3 in February 2019.

430 Monthly SS counts correlations with SST, SST Anomaly (both in 3.4 and 1+2), ONI, MEI, AMO and
431 PDO through the whole time series (1954-2017) were poor; these had a correlation r^2 averaging
432 0.020 and a negative linear regression slope. It was observed that on the long run, there is not
433 strong correlation between SS and PDO, MEI, ONI and SST Anomaly in 3.4, where the r^2 were: 0.043,
434 0.029, 0.040 and 0.021 respectively. In the case of region 1+2, the correlation was even poorer:
435 <0.005 .

436

437 The series of correlations at different lag times (6, 12, 24, 36 and 48 months) gave a response time of
438 12-24 months for all indexes, except for AMO (48 months), which align to what was previously
439 reported by Kristoufek, (2017), and Huo and Xiao (2016); i.e., in general the highest correlation
440 coefficients were found at that lag time (Table 1).

441

442 Changes of the SS could bring climate impact; there is a lengthy discussion about the effect on
443 climate change due to SS cycles. Gil-Alana et al. (2014) have found no significant statistical relation



444 between sun spots and global temperature; however, van Loon et al. (2007) suggested that even
445 though SS cycles produce weak changes on Solar Irradiation (SI) of about 0.07% according to Gray et
446 al. (2010); still, these can produce decadal and millennial impact on global thermohaline circulation
447 (Bond et al. 2001, Gray et al., 2016), due chiefly to UV energy fluctuation (Ineson et al., 2014). The
448 changes in UV (<100 nm to 350 nm) and near infrared (>800 nm to >1000 nm) are larger than in the
449 visible radiation (>350 nm-800 nm) and could have an important impact on global climate (Ermolli et
450 al. 2013); therefore, it is reasonable to deem some impact on the studied oceanographic indexes.
451 Recent data (Solar Radiation and Climate Experiment Satellite) suggest that the variability of UV
452 radiation during the declining phase of cycle 23 was larger than previous estimates (Harder et al.,
453 2009 and Haigh et al., 2010). Despite these small SI variations between the peaks and valleys of the
454 SS cycles, as 1) the total SI integrates over all the wavelengths, and 2) considering the huge heat
455 capacity of the seawater; these fluctuations give a strong possibility of increasing heat even at this
456 low SI variation. Also, there has been found that UV radiation penetrates down to 75-100 m depth of
457 the water column (Smyth, 2011), even though its variation is around 8% of total SI during the highs-
458 lows of SS cycles.

459

460 **Individual SS cycles (19-24).** The SSTs correlations against individual SS cycles in regions 3.4 and 1+2
461 (Fig. 2) analysis rendered some insights; thus, in cycles 19, 21 and 23 were found the higher
462 correlations but variable in the region 3.4, up to 0.219 (SS# 23). The lag response time was 12-36
463 months in all cycles except 19, in line with Kristoufek, (2017) and Huo and Xiao (2016) reports. In
464 region 1+2, linear correlation r^2 was <0.0675 (SS# 19), and inconstant between cycles. Up to sixth-
465 degree polynomial correlation of SS against SST, SST Anomaly and other indexes were attempted
466 with equally poor correlation.

467



468 SS was correlated with anomalies SST (ERRSV4) in 3.4 and 1+2 (Fig. 3) in every cycle and did not have
469 a better r^2 than 0.396, for cycle 19 (in 1+2). Correlation factor r^2 showed high variability as well the
470 response time response (12-36 months). Correlation coefficient r^2 went up to 0.289 (in 3.4) and
471 0.396 (in 1+2) occurring in cycles 19 and 23 respectively, within the cold phase of PDO: 1955-1978
472 and 2000-present. In the period 1990-2016 in which occurred the two strongest El Niño (1997-1998
473 and 2015) and La Niña (2000-2002 and 2010-2012) in 1+2 region, still the SST Anomaly vs SS
474 correlation (r^2 of 0.127) was poorer than in 3.4 The slopes of the linear correlation were basically
475 positive for 3.4 and negative for 1+2. In general, in 1+2 there was found a more inconstant and lower
476 correlation than in 3.4. This is thought due to basically high seasonal and interannual variability of
477 oceanographic coastal conditions (Ormaza-González and Cedeño, 2017) that obscures the
478 correlation with SS. In 3.4, correlation is better, although it is still affected by fluctuation of regional
479 oceanographic and meteorological conditions expressed through some indexes; e.g., the Southern
480 Oscillation Index (Rasmussen and Carpenter, 1982; Barnston, 2015).

481

482 During the cycle 24, the ONI index was highly correlated to SS (Fig. 5), registering a r^2 up to 0.2510
483 $p < 1.8E^{-07}$) with a positive slope; which gives degree of correlation between high and moderate. It is
484 noteworthy to mention that in this cycle ONI reached 2.6C (Nov-Dec-Jan 2015/2016) and -1.7C (Oct-
485 Nov-Dec 2010). In cycles 20-21 the r^2 was low ($r^2 < 0.04$, $p = 0.02$); however, from 22 to 24, r^2
486 increased from 0.131 ($p < 0.00006$) to 0.251. The variability of the correlation can be ascribed also
487 to:

488 1) fluctuation of SS number from one month to another;

489 2) regional meteorological conditions (particularly cloudiness), ocean surface currents that transport
490 heat as Kelvin waves (Gill, 1982), SOI (<http://www.cpc.ncep.noaa.gov/data/indices/soi>), etc. that in
491 turn affects the SSTs; and,



492 3) the way ONI is obtained: is the average of three successive months, but it has displacing reference
493 period of 30 years; thus, for the period 1950-1955, the reference period is 1936-1965; for 1956-
494 1960; 1941-1970 and so on. The EERSv4 uses the period 1981-2010, in which 3 very strong El Niño
495 and many others has occurred; thus, the reference moving period of 30 years will slightly affect the
496 ONI index somehow (Lindsey, 2013).

497

498 The PDO is an index (Fig. 5) for interdecadal oscillation alike AMO; it seemed to respond in 36-48
499 months to SS cycle showing a high degree of correlation coefficient r of 0.625 (SS#19) and 0.766 (SS#
500 24); for cycles 20-23: 0.467-0.508, linearly correlated with fair-good degree and positive slope
501 (except in SS# 20). A better fit occurred in the cycles 19 and 24, which have the highest and lowest
502 SS peak of the six cycles analyzed (Fig. 10), both are in the cold phase of the PDOs. The AMO index
503 (Fig. 6) gave a variable correlation, from a weak r^2 of 0.130 ($p=0.00001$) to strong 0.490
504 ($p<<0.00001$) with a response time of 48 months for cycles 23 and 20 respectively. Gray et al. (2016)
505 reported 36-48 months lag for mean-sea-level pressure in the North Atlantic in a study of 32 SS
506 cycles. The slopes of the PDO and AMO linear regression curves are negative and positive
507 respectively in cycle 21 and 22, but in concordance in 19, 20, 23 and 24 during cold phase PDO.
508 These two interdecadal oscillations proved to be correlated to SS; however, the PDO showed higher
509 correlation. Perhaps, since the North Pacific Ocean basin has a larger area than the North Atlantic;
510 there is higher heat storage capacity in the first.

511

512 The analysis through the ascending and descending phases of each cycle rendered clearer results.
513 The SSTs in 1+2 showed higher correlation with r up to 0.2052 in the ascending phases; in the
514 descending phase r was below 0.067 0.259; however, the response time and slope of the linear
515 correlation curves did not show a specific pattern. In region 3.4, there was a high degree of
516 correlation: 0.8699 (SS# 24), 0.6089 (SS# 22), 0.5736 (SS# 19) and 0.5559 (SS# 23), at ascending



517 phase of the cycles (except SS# 20 and 24). The response time was 36 months. Slopes were negative
518 and positive during warm (SS# 20-22) and cold (SS# 19, 23, 24) PDO phases respectively. The highest
519 r^2 : 0.870 in the descending phase in the cycle 24 coincided with the strongest El Niño (2015) and the
520 second highest (SS# 22) with two consecutive strong El Niño 1991-1995, the third with el Niño 1955-
521 1957, and finally the fourth during 1997-1998 warm event. It seems that short time expressions of
522 SS cycles, either at the beginning of their ascending or descending phases, have a trigger effect on
523 the SSTs. This was observed through the polynomial regression curves (Fig. 12) that were found for
524 each SS cycle. The polynomial curves of order 6 were fitted with an average $r^2 > 0.89$ ($p \leq 0.001$).
525 However, a response time of 24-36 months seems to occur at the low or high plateau of the cycles
526 (Fig. 12), then the event is the strongest. Thus, El Niño 1957-1958 (SS# 19), 1965-1966 (SS# 20), 1981-
527 1982 (SS# 21), 1987-1988 and 1991-1992 (SS# 22), 1997-1998 (SS# 23), 2015-2016 (SS# 24). On the
528 other hand, the cold events La Niña tends to occur after an El Niño at the middle of the ascending
529 phases (1988-1989, 1999-2001, 2010-2012) or when approaching the minimum of the cycles (1973-
530 1974, 1975-1975; 1995-1996, 1917-1918). The so called equatorial Pacific neutral conditions in 3.4
531 (see, https://iridl.ldeo.columbia.edu/maproom/ENSO/ENSO_Info.html), seems to span a longer
532 period after La Niña, vice versa after El Niño.

533

534 The ENSO indexes ONI and MEI also showed strong correlation associated to the ascending phase of
535 the SS cycles, with a lag time of 24-36 months. In four cycles, correlation coefficient r varied from
536 0.3913 (fair) to 0.9038 (strong) in the ascending phase with a positive slope of the linear regression
537 curve. The three highest r match dates of strong El Niño 87-89, 55-57 and 97-98 with positive slope
538 and ascending phase. During the descending phase, the correlation coefficients were lower and
539 ranged from 0.6082 to 0.2938, all of them with lag time 0-12 months and positive slope. In this
540 exercise, it was also found that warm events tend to occur in the ascending phase or at the top of
541 the cycle and have a delay time of 36 months, which was reported also by Huo and Xiao (2016),



542 whilst cold events are associated to a descending phase but with a quicker response time: 0-12

543 months, except La Niña 1988-1989 and 2010-2012.

544

545 Similarly, for MEI, r^2 ranged from : 0.784 (SS# 19) to 0.222 (SS# 21), in the ascending phase and lag

546 time 12-48 months (except SS# 23 and 24). During the descending phase, the correlation r^2

547 coefficients were lower and varied from 0.321 (SS# 24) to 0.143 (SS# 23) with positive slope and

548 quicker lag time 0-12 months. The index MEI resembles similar pattern as ONI; lower correlation

549 may arise as MEI take into consideration six variables that all together may mask the signal from sun

550 activity.

551

552 On a longer time scale, the interdecadal oscillation of the Pacific (PDO) and Atlantic (AMO) were

553 strongly correlated to SS. The PDO (Fig 10) was linearly correlated with r^2 coefficient, ranging from

554 0.7677 to 0.2854 in the ascending phase with lag time 24-36 months, as reported by Huo and Xiao

555 (2016), with positive slopes in cold phase PDO (cycles 19, 23 and 24) and the contrary in warm PDO

556 (cycles 21 and 22); whilst cycle 20 was a sort of transitioning period between the PDO phases. The r^2

557 of AMO (Fig. 11) with individual SS cycles varied from 0.160 to 0.700. Similarly, the response time

558 was 24-48 months. These results correspond with van Loon et al. (2007), who established that even a

559 low change in the sun activity (SI) could produce decadal and millennial time scales affecting

560 thermohaline circulation (Bond et al. 2001, Gray et al., 2016), which in turn is reflected by PDO and

561 by the AMO index, which is somehow in opposite phase to PDO (Enfield et al., 2001; Condrón et al.,

562 2005).

563 Recently, after the second quarter of 2018, many models and researchers are projecting El Niño to

564 occur sometimes in late northern hemisphere summer (see:

565 <http://www.bom.gov.au/climate/enso/>); but it did not occur. Then, the projections passed to the



566 beginning of autumn (<http://www.cpc.ncep.noaa.gov/products/precip/CWlink/MJO/enso.shtml>);
567 similarly, it did not happen. Now, on the third week of September, it is pronounced to occur in late
568 autumn, but with fewer models asserting the event. Most models seem to be failing to provide a
569 consistent projection. Probably, this is because, there has been two re-cooling processes in all El
570 Niño areas, that keep the ONI index within the realm of ENSO neutrality (-0.5C to 0.5C). The PDO
571 index have been averaging -0.53, and it is in its cold phase
572 (<https://www.ncdc.noaa.gov/teleconnections/pdo/>). Sun spots have been at very low numbers, with
573 some weeks without any. During 2017 the average smoothed SS counts per month was 21.8, and for
574 2018 is 8.5, with just 1.6 in July (<http://www.sws.bom.gov.au/Solar/1/6>) with expected counts to
575 decrease to 5.3 in February 2019. Probably, there will not be an event El Niño during 2018 or at least
576 little chance according to present results.

577

578 **Data availability.** All data are publicly available on the Web (see Material and Methods).

579

580 **Author contributions.** Franklin Isaac Ormaza-González led and oversaw the whole project. He
581 conceptualized the hypothesis, researched the literature, designed the material and methods, and
582 wrote the paper in all its stages. María Esther Espinoza-Celi looked for and retrieved all data and
583 information, run statistical and spectral analysis, organized results, and designed graphs. She
584 designed the poster presentation.

585

586 **Acknowledgements.** Authors are grateful to ESPOL authorities whose supported research allotting
587 time and financial resources to present paper in the “4TH INTERNATIONAL SYMPOSIUM: THE
588 CLIMATE CHANGE EFFECTS ON THE WORLD OCEANS” held in Washington DC, 4-8 June 2018, also



589 The National Chamber of Fisheries of Ecuador support is acknowledged. Work on the English by

590 Dafne Vera-Mosquera is indeed appreciated.



591 **References**

- 592 1. Allan, R.J., and Ansell, T.: A new globally complete monthly historical gridded mean sea level
593 pressure dataset (HadSLP2): 1850-2004, *J. Climate*, 19, 5816-5842, 2006.
- 594 2. Barnston, A.: Why are there so many ENSO indexes, instead of just one?
595 [https://www.climate.gov/news-features/blogs/enso/why-are-there-so-many-enso-indexes-](https://www.climate.gov/news-features/blogs/enso/why-are-there-so-many-enso-indexes-instead-just-one)
596 [instead-just-one](https://www.climate.gov/news-features/blogs/enso/why-are-there-so-many-enso-indexes-instead-just-one) (last access: 15 March 2018), 2015.
- 597 3. Bond, G. G., Kromer, B., Beer, J., Muscheler, R., Evans, M., Showers, W., Hoffmann, S., Lotti-
598 Bond, R., Hajdas, I., and Bonani, G.: Persistent Solar Influence on North Atlantic Climate
599 During the Holocene, *Science*, 294, 2130–2136, 2001.
- 600 4. Busalacchi, A.J., Takeuchi, K., and O'Brien, J.J.: Interannual variability of the equatorial
601 Pacific-revisited, *J. Geophys. Res.*, 88, 7551-7562, 1983.
- 602 5. Chen, X., and Tung, K.K.: Varying planetary heat sink led to global-warming slowdown and
603 acceleration, *Science*, 345, 897–903, doi:10.1126/science.1254937, 2014.
- 604 6. Clette, F., Svalgaard, L., Vaquero, J. M., and Cliver, E. W.: Revisiting the Sunspot Number,
605 *Space Sci. Rev.*, 186, 35-103, doi: 10.1007/s11214-014-0074-2, 2014.
- 606 7. Clutz, R.: Global ocean cooling in September (2017),
607 <https://rclutz.wordpress.com/2017/10/26/global-ocean-cooling-in-september/> (last access:
608 30 October 2017), 2017.
- 609 8. Compo, G.P., and Sardeshmukh, P.D.: Oceanic influences on recent continental warming,
610 *Clim. Dynam.*, 32, 333-342, doi:10.1007/s00382-008-0448-9, 2009.
- 611 9. Condrón, A., DeConto, R., Bradley, R. S., and Juanes, F.: Multidecadal North Atlantic climate
612 variability and its effect on North American salmon abundance, *J. Geophys. Res. Lett.*,
613 32L23703, doi:10.1029/2005GL024239, 2005.
- 614 10. Dicke, R.H.: Is there a chronometer hidden deep in the Sun?, *Nature*, 276, 676-680, 1978.
- 615 11. Eddy, J. A.: The Maunder Minimum, *Science*, 192 (4245), 1189–1202,
616 doi:10.1126/science.192.4245.1189, 1976.



- 617 12. Enfield, D.B., Mestas-Nuñez, A.M., and Trimble, P.J.: The Atlantic multidecadal oscillation
618 and its relation to rainfall and river flows in the continental US, *J. Geophys. Res. Lett.*, 28,
619 2077–2080, doi:10.1029/2000GL012745, 2001.
- 620 13. Ermolli, I., Matthes, K., Dudok de Wit, T., Krivova, N. A., Tourpali, K., Weber, M., Unruh, Y. C.,
621 Gray, L., Langematz, U., Pilewskie, P., Rozanov, E., Schmutz, W., Shapiro, A., Solanki, S. K.,
622 and Woods, T.N.: Recent variability of the solar spectral irradiance and its impact on climate
623 modelling, *Atmos. Chem. Phys.*, 13, 3945–3977, doi:10.5194/acp-13-3945-2013, 2013.
- 624 14. Fasullo, J., and Nerem, R.: Interannual variability in global mean sea level estimated from the
625 CESM Large and last millennium ensembles, *Water*, 8, 491, doi:10.3390/w8110491, 2016.
- 626 15. Fröhlich C.: *Solar Constant and Total Solar Irradiance Variations*, edited by: Richter, C.,
627 Lincot, D., Gueymard C.A., Solar Energy, Springer, New York, NY, 2013.
- 628 16. Gil, L.A., Yaya, O.S., and Shittu, O.I.: Global temperatures and sunspot numbers. Are they
629 related? *Physica A.*, 396, 42–50, 2014.
- 630 17. Gill, A. E.: *Atmosphere–Ocean Dynamics*, International Geophysics Series, Academic Press,
631 edited by: Donn, W. L., 30, 662 pp., eBook ISBN: 9780080570525, Paperback
632 ISBN: 9780122835223, 1982.
- 633 18. Glantz, M. H.: *Once burned, twice shy? Lessons learned from the 1997-1998 El Niño*, The
634 Unite Nations University, 294 pp, 2001.
- 635 19. Gray, L. J., Beer, J., Geller, M., Haigh, J. D., Lockwood, M., Matthes, K., Cubasch, U.,
636 Fleitmann, D., Harrison, G., Hood, L., Luterbacher, J., Meehl, G. A., Shindell, D., van Geel, B.,
637 and White, W.: Solar influences on climate, *Rev. Geophys.*, 48, RG4001,
638 doi:10.1029/2009RG000282, 2010.
- 639 20. Gray, L. J., Woollings, T. J., Andrews, M., and Knight, J.: Eleven-year solar cycle signal in the
640 NAO and Atlantic/European blocking, *Q. J. Roy. Meteor. Soc.*, 142, 1890–1903,
641 doi:10.1002/qj.2782, 2016.



- 642 21. Hady, Ahmed A.: Deep solar minimum and global climate changes. *J. Advanced Res* (ISSN:
643 2090-1232), Vol: 4, Issue: 3, Page: 209-214. 2013 <https://doi.org/10.1016/j.jare.2012.11.001>.
- 644 22. Haigh, J. D., Winning, A.R., Toumi, R., and Harder, J. W.: An influence of solar spectral
645 variations on radiative forcing of climate, *Nature*, 467, 696–699, 2010.
- 646 23. Harder, J. W., Fontenla, J. M., Pilewskie, P., Richard, E. C., and Woods, T. N.: Trends in solar
647 spectral irradiance variability in the visible and infrared, *J. Geophys. Res. Lett.*, 36L07801,
648 2009.
- 649 24. Hathaway, D. H.: The Solar Cycle, *Living Rev. Sol. Phys.*, 12, 4, doi:10.1007/lrsp-2015-4, 2015.
- 650 25. Henley, B.J., Gergis, J., Karoly, D.J., Power, S., Kennedy, J., and Folland, C.K.: A Tripole Index
651 for the Interdecadal Pacific Oscillation, *Clim. Dynam.*, 45, 3077, doi:10.1007/s00382-015-
652 2525-1, 2015.
- 653 26. Horning, N., Russell, C., and Goetz, S.: Energy from the Sun to Earth's Surface. In Chapter 2:
654 Earth's Radiation Balance and the Global Greenhouse,
655 https://people.ucsc.edu/~mdmccar/migrated/ocea80b/public/lectures/lect_notes_1/03_En
656 [ergy_Balance_MDM_11F.pdf](https://people.ucsc.edu/~mdmccar/migrated/ocea80b/public/lectures/lect_notes_1/03_En) (last access: 25 April 2018), 2003.
- 657 27. Huang, B., Banzon, V.F., Freeman, E., Lawrimore, J., Liu, W., Peterson, T.C., Smith, T.M.,
658 Thorne, P. W., Woodruff, S. D., and Zhang, H. M.: Extended Reconstructed Sea Surface
659 Temperature version 4 (ERSST.v4): Part I. Upgrades and intercomparisons, *J. Climate*, 28,
660 911–930, doi:10.1175/JCLI-D-14-00006, 2014.
- 661 28. Huang, B., Thorne, P.W., Banzon, V.F., Boyer, T., Chepurin, G., Lawrimore, J.H., Menne, M.J.,
662 Smith, T. M, Vose, R. S., and Zhang, H. M.: Extended Reconstructed Sea Surface
663 Temperature, Version 5 (ERSSTv5): Upgrades, Validations, and Intercomparisons, *J.*
664 *Climate*, 30, 8179–8205, doi:10.1175/JCLI-D-16-0836.1, 2017.
- 665 29. Huo, W.J., and Xiao, Z.N.: The impact of solar activity on the 2015/16 El Niño event,
666 *Atmospheric and Oceanic Science Letters*, doi: 10.1080/16742834.2016.1231567, 2016.



- 667 30. Ineson, S., Maycock, A. C., Gray, L. J., Scaife, A. A., Dunstone, N. J., Harder, J. W., Knight, J. R.,
668 Lockwood, M., Manners, J. C., and Wood, R. A.: Regional climate impacts of a possible future
669 grand solar minimum, *Nat. Commun.*, 6, 7535, doi:10.1038/ncomms8535, 2015.
- 670 31. Knauss, J. A.: Measurements of the Cromwell current, *Deep-Sea Res.*, 6, 265-286,
671 doi.org/10.1016/0146-6313(59)90086-3, 1959.
- 672 32. Kopp, G., and Lean, J. L.: A new, lower value of total solar irradiance: Evidence and climate
673 significance, *J. Geophys. Res. Lett.*, 38L01706, doi:10.1029/2010GL045777, 2011.
- 674 33. Kristoufek, L.: Has global warming modified the relationship between sun spot numbers and
675 global temperatures? *Physica A.*, 468, 351-358, doi:10.1016/j.physa.2016.10.089, 2017.
- 676 34. Labitzke, K., Austin, J., Butchart, N., Knight J., Takahashi, M., Nakamoto, M., Nagashima, T.,
677 Dorothy, J., and Williams, V.: The global signal of the 11-year solar cycle in the stratosphere:
678 Observations and model results, *J. Atmos. Terr. Phys.*, 64, 203-210, doi:10.1016/S1364-
679 6826(01)00084-0, 2002.
- 680 35. Lindsey, R.: Climate and Earth's Energy Budget. In NASA Earth Observatory,
681 <https://earthobservatory.nasa.gov/Features/EnergyBalance/> (last access: 25 April 2018),
682 2009.
- 683 36. Lindsey, R.: In Watching for El Niño and La Niña, NOAA Adapts to Global Warming,
684 [https://www.climate.gov/news-features/understanding-climate/watching-el-ni%C3%B1o-](https://www.climate.gov/news-features/understanding-climate/watching-el-ni%C3%B1o-and-la-ni%C3%B1a-noaa-adapts-global-warming)
685 [and-la-ni%C3%B1a-noaa-adapts-global-warming](https://www.climate.gov/news-features/understanding-climate/watching-el-ni%C3%B1o-and-la-ni%C3%B1a-noaa-adapts-global-warming) (last access: 25 April 2018), 2013.
- 686 37. Liu, F., Chai, J., Huang, G., Liu, J., and Chen, Z.: Modulation of decadal ENSO-like variation by
687 effective solar radiation, *Dynam. Atmos. Oceans*, 72, 52-61, ISSN: 0377-0265, 2015.
- 688 38. Lockwood, M.: Solar change and climate: an update in the light of the current exceptional
689 solar minimum, *P. Roy. Soc. A-Math Phys.*, 466, 303-329, 2010.
- 690 39. Lockwood, M.: Reconstruction and prediction of variations in the open solar magnetic flux
691 and interplanetary conditions, *Living Rev. Sol. Phys.*, 10, 4, 2013.



- 692 40. Mantua, N. J., Hare, S. R., Zhang, Y., Wallace, J. M., and Francis, R. C.: A Pacific interdecadal
693 climate oscillation with impacts on salmon production, *B. Am. Meteorol. Soc.*, 78, 1069–
694 1079, 1997.
- 695 41. Mantua, N. J., and Hare, S. R.: The Pacific Decadal Oscillation, *J. Oceanogr.*, 58, 35–44, 2002.
- 696 42. McKinley, G. A., Takahashi, T., Buitenhuis, E., Chai, F., Christian, J. R., Doney, S. C., Jiang, M.-
697 S., Lindsay, K., Moore, J.K., Le Quéré, C., Lima, I., Murtugudde, R., Shi, L., and Wetzel, P.:
698 North Pacific carbon cycle response to climate variability on seasonal to decadal timescales,
699 *J. Geophys. Res.*, 111, C07S06, doi:10.1029/2005JC003173, 2006.
- 700 43. Montecino, V., and Lange, C. B.: The Humboldt Current System: Ecosystem components and
701 processes, fisheries, and sediment studies, *Prog. Oceanogr.*, 83, 65-79, 2009.
- 702 44. Monteith, J. L.: Solar Radiation and Productivity in Tropical Ecosystems, *J. App. Ecol.*, 9, 747-
703 66, doi:10.2307/2401901, 1972.
-
- 704 45. Montgomery, D. C., Peck, E. A. and Vining, G. G. (2001). *Introduction to Linear Regression*
705 *Analysis*. 3rd Edition, New York, New York: John Wiley & Sons.
- 706 46. Mörner, N.-A.: The Approaching New Grand Solar Minimum and Little Ice Age Climate
707 Conditions, *Natural Science*, 7, 510-518, doi: 10.4236/ns.2015.711052, 2015.
- 708 47. Newman, M., Compo, G. P., and Alexander, M. A.: ENSO-forced variability of the
709 Pacific decadal oscillation, *J. Climate*, 16, 3853-3857, doi: 10.1175/1520-
710 0442(2003)016<3853: EVOTPD>2.0.CO;2., 2003.
- 711 48. Ormaza-González, F.I., and Cedeño, J.: Coastal El Niño 2017 or Simply: The Carnival Coastal
712 Warming Event? *MOJ Ecology & Environmental Sciences*, 2, 00054, doi:
713 10.15406/mojes.2017.02.00054, 2017.
- 714 49. Ormaza-González, F. I., and Sánchez, E.: Cálculo computacional del flujo de energía solar
715 sobre el océano y su aplicación a la zona ecuatorial, *Rev. Ciencias del Mar y Limnología (INP-*
716 *Ecuador)*, 2(1), 27-54, ISSN 1390-5767, 1983.



- 717 50. Ormaza-González, F. I., Mora, A., Bermúdez, R. M., Hurtado, M. A., Peralta, M. R., and
718 Jurado, V. M.: Can small pelagic fish landings be used as predictors to high frequency
719 oceanographic fluctuations in the 1-2 El Niño region? *Adv. Geosci.*, 42, 61–72,
720 doi:10.5194/adgeo-42-61-2016, 2016a.
- 721 51. Ormaza-González, F. I., Mora, A., and Bermúdez, R. M.: Relationships between tuna catch
722 and variable frequency oceanographic conditions, *Adv. Geosci.*, 42, 83–90,
723 doi:10.5194/adgeo-42-83-2016, 2016b.
- 724 52. Rasmussen, E. M., and Carpenter, T. H.: Variations in tropical sea surface temperature and
725 surface wind fields associated with the Southern Oscillation/El Niño, *Mon. Weather*
726 *Rev.*, 110, 354-384, 1982.
- 727 53. Scafetta, N.: Global temperatures and sun spot numbers. Are they related? Yes, but non-
728 linearly. A reply to Gil-Alana et al. (2014), *Physica A.*, 413, 329-342, doi:
729 10.1016/j.physa.2014.06.047, 2014.
- 730 54. Shindell, D. T., Schmidt, G. A., Mann, M. E., Rind, D., and Waple, A.: Solar Forcing of Regional
731 Climate Change During the Maunder Minimum, *Science*, 294 (5549), 2149-2152, doi:
732 10.1126/science.1064363, 2001.
- 733 55. Schlesinger, M. E., and Ramankutty, N.: An oscillation in the global climate system of period
734 65–70 years, *Nature*, 367, 723–726, doi:10.1038/367723a0., 1994.
- 735 56. Smyth, T. J. 2011. Penetration of UV irradiance into the global ocean. *J. Geophys.*
736 *Res.*, 116C11020, doi:10.1029/2011JC007183.
- 737 57. Trenberth, K.E., Fasullo, J.T., and Balmaseda, M.A.: Earth's Energy Imbalance, *J. Climate*, 27,
738 3129–3144, doi:10.1175/JCLI-D-13-00294.1, 2014.
- 739 58. van Oldenborgh, G. J., te Raa, L. A., Dijkstra, H. A., and Philip, S. Y.: Frequency- or amplitude-
740 dependent effects of the Atlantic meridional overturning on the tropical Pacific Ocean,
741 *Ocean Sci.*, 5, 293-301, doi:10.5194/os-5-293-2009, 2009.



- 742 59. van Loon, H., Meehl, G. A., and Shea, D. J.: Coupled air-sea response to solar forcing in the
743 Pacific region during northern winter, *J. Geophys. Res.*, 112D02108,
744 doi:10.1029/2006JD007378, 2007.
- 745 60. Wang, G., Cheng, L., Abraham, J., and Li, C.: Consensuses and discrepancies of basin-scale
746 ocean heat content changes in different ocean analyses, *Clim. Dynam.*, doi:10.1007/s00382-
747 017-3751-5, 2017.
- 748 61. Wenjuan, H., and XIAO, Z.: The impact of solar activity on the 2015/16 El Niño event,
749 *Atmospheric and Oceanic Science Letters*, doi:10.1080/16742834.2016.1231567, 2016.
- 750 62. White, W. B., Lean, J., Cayan, D. R., and Dettinger, M. D.: Response of global upper ocean
751 temperature to changing solar irradiance, *J. Geophys. Res.*, 102(C2), 3255–3266,
752 doi:10.1029/96JC03549, 1997.
- 753 63. Wolter, K., and Timlin, M.S.: Monitoring ENSO in COADS with a seasonally adjusted principal
754 component index, *Proceedings of the 17th Climate Diagnostics Workshop*, 52-57, Norman,
755 OK, 1993.
- 756 64. Wolter, K., and Timlin, M. S.: Measuring the strength of ENSO events - how does 1997/98
757 rank? *Weather*, 53, 315-324, 1998.
- 758 65. Wolter, K., and Timlin, M. S.: El Niño/Southern Oscillation behaviour since 1871 as diagnosed
759 in an extended multivariate ENSO index (MEI.ext), *Int. J. Climatol.*, 31, 1074–1087,
760 doi:10.1002/joc.2336, 2011.
- 761 66. Yamakawa, S., Makoto, I., and Ramasamy, S.: Relationships between solar activity and
762 variations in SST and atmospheric circulation in the stratosphere and troposphere, *Quatern.*
763 *Int.*, 397, 289-299, 2016.
- 764 67. Yim, B. Y., Noh, Y., Yeh, S. -W., Kug, J. -S., Min, H. S., and Qiu, B.: Ocean mixed layer
765 processes in the Pacific Decadal Oscillation in coupled general circulation models, *Clim.*
766 *Dynam.*, 41, 1407–1417, doi: 10.1007/s00382-012-1630-7, 2013.



- 767 68. Yoon, J., and Yeh, S. -W.: Influence of the Pacific Decadal Oscillation on the Relationship
768 between El Niño and the Northeast Asian Summer Monsoon, *J. Climate*, 23, 4525–4537,
769 doi:10.1175/2010JCLI3352.1, 2010.
- 770 69. Yuan, Y., and Yan, H.: Different types of La Niña events and different responses of the
771 tropical atmosphere, *Chinese Sci. Bull.*, 58, 406–415, doi:10.1007/s11434-012-5423-5, 2012.
- 772 70. Zhang, Y., Wallace, J. M., and Battisti, D. S.: ENSO-like Interdecadal Variability: 1900–93, *J.*
773 *Climate*, 10, 1004-1020, 1997.
- 774 71. Zheng, F., Fang, X.-H., Zhu, J., Yu, J.-Y., and Li, X.-C.: Modulation of Bjerknes feedback on the
775 decadal variations in ENSO predictability, *J. Geophys. Res. Lett.*, 43, 560–568,
776 doi:10.1002/2016GL07163, 2016.
- 777 72. Zhou, J., and Tung, K. -K.: Solar Cycles in 150 Years of Global Sea Surface Temperature Data,
778 *J. Climate*, 23, 3234-3248, 2010.
- 779 73. Zong, Z., Yong, L., and Jian, H.: Effects of Sunspot on the Multi-Decadal Climate Projections,
780 *Advances in Climate Change Research*, 5, 51-56, doi:10.3724/SP.J.1248.2014.051, 2014.
- 781



782

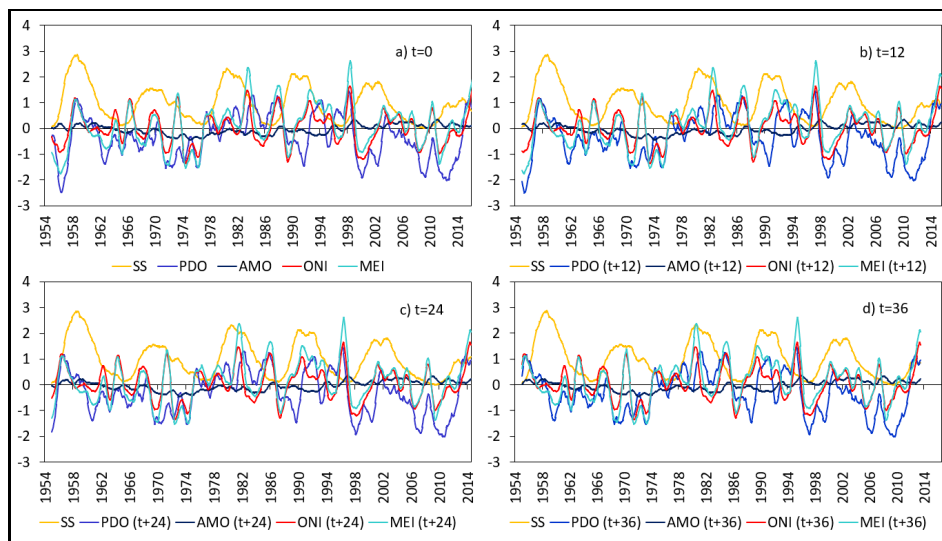
783 **Table 1.** Linear correlations r^2 and p-values between SS monthly counts and PDO, MEI, ONI, AMO,
 784 SST and SST Anomaly in 1+2, and 3.4. The time series April 1954 to December 2017. Values in yellow
 785 background mean negative slopes of the linear regression curves. Pink shading cells are $p > 0.05$. Red:
 786 r^2 values below 0.001.

Variable		T+0	(t+6)	(t+12)	(t+24)	(t+36)	(t+48)
PDO	r^2	0.00	0.02	0.04	0.04	0.03	0.02
	p-value	3.83E-01	1.75E-04	1.94E-07	1.26E-08	2.07E-06	3.11E-05
MEI	r^2	0.01	0.02	0.03	0.02	0.01	0.00
	p-value	2.58E-02	9.68E-05	2.55E-06	1.63E-05	1.51E-02	9.30E-01
ONI	r^2	0.01	0.03	0.04	0.03	0.01	0.00
	p-value	2.22E-03	4.93E-06	2.11E-07	1.91E-06	4.00E-03	4.13E-01
AMO	r^2	8.66E-05	8.30E-04	9.66E-04	2.89E-03	1.39E-02	1.89E-02
	p-value	7.97E-01	4.28E-01	3.94E-01	1.44E-01	1.45E-03	2.21E-04
SST 1+2	r^2	2.54E-04	1.61E-03	3.08E-05	2.92E-06	3.04E-04	1.26E-03
	p-value	6.61E-01	2.71E-01	8.80E-01	9.63E-01	6.37E-01	3.44E-01
SSTA 1+2	r^2	0.00	0.00	0.00	0.00	0.00	0.00
	p-value	7.14E-01	1.67E-01	3.37E-01	2.57E-01	8.13E-01	3.73E-01
SST 3.4	r^2	0.00	0.01	0.01	0.01	0.00	0.00
	p-value	2.78E-01	5.93E-03	1.07E-03	1.32E-03	6.48E-02	9.10E-01
SSTA 3.4	r^2	0.00	0.01	0.02	0.02	0.01	0.00
	p-value	1.45E-01	2.25E-03	8.23E-05	1.23E-04	2.45E-02	9.79E-01

787

788

789 **Fig. 1.** Behaviour of monthly counts SS, ONI, MEI, PDO and AMO. The indexes start at t= 0, 12 and
 790 36 months (panels a, b, c and d respectively). The SS series starts at t=0 in the four panels. The
 791 vertical axe gives the values for the indexes and SS numbers (multiply by 100).

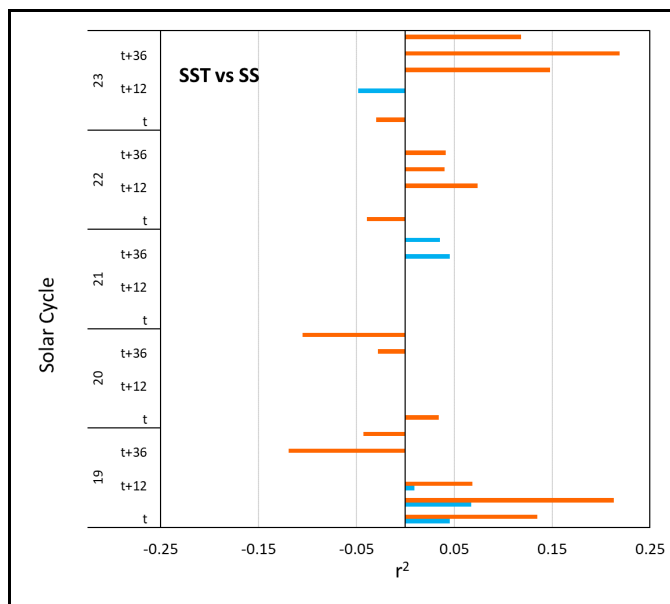


792

793



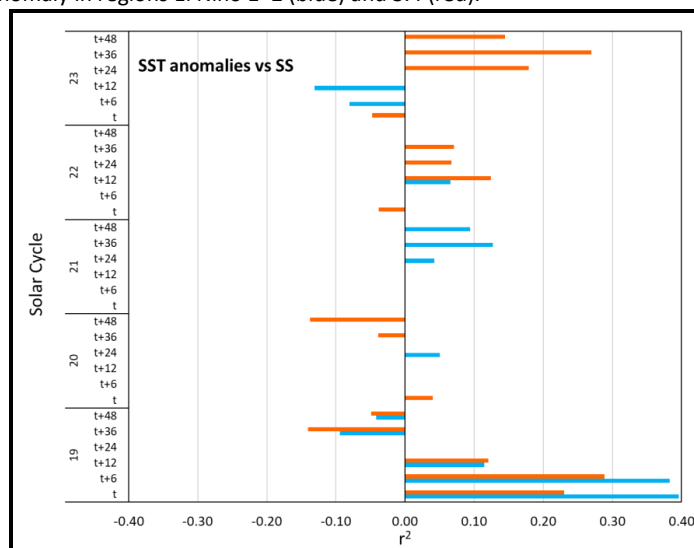
794 **Fig. 2.** Linear regression correlation coefficient r^2 ($p < 0.05$) of SS monthly counts for cycles 19-24
795 against SST in regions El Niño 1+2 (blue) and 3.4 (red).



796



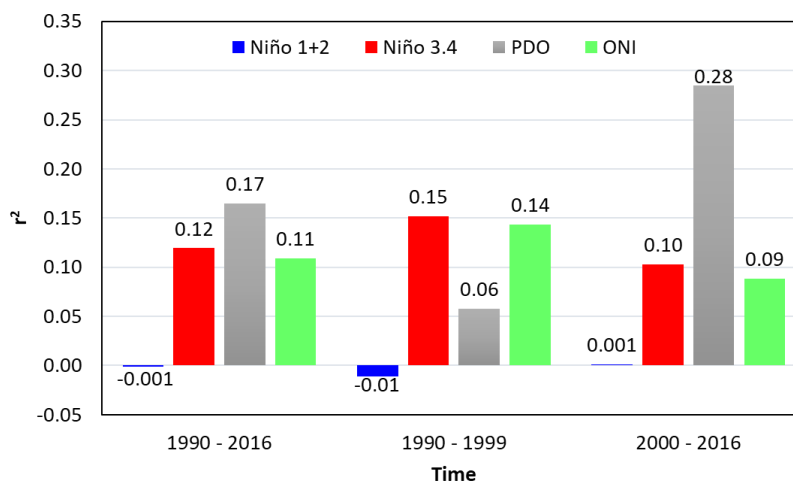
797 **Fig. 3.** Linear regression correlation coefficient r^2 ($p < 0.05$) of SS monthly counts of cycles 19-24
 798 against SST Anomaly in regions El Niño 1+2 (blue) and 3.4 (red).



799

800

801 **Fig. 4.** Linear regression correlation coefficient r^2 ($p < 0.05$) of SS monthly counts against SST Anomaly
 802 in regions El Niño 1+2 (blue) and 3.4 (red) and indexes PDO (grey) and ONI (green) through three
 803 time periods.



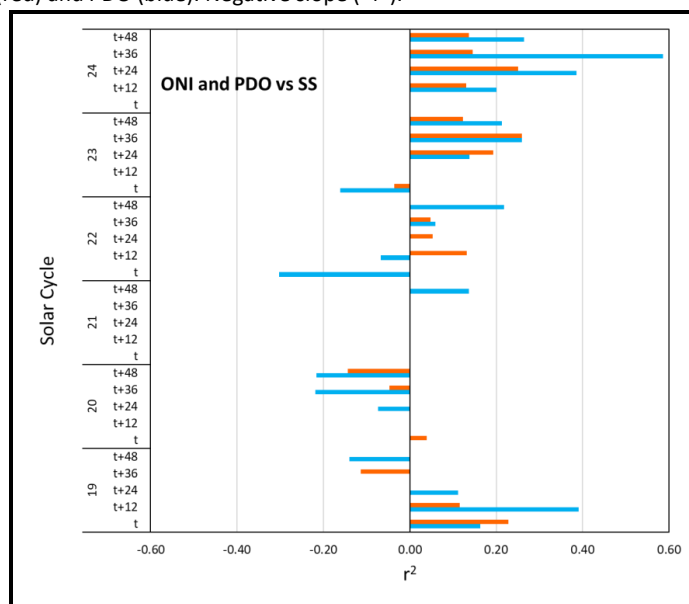
804

805

806

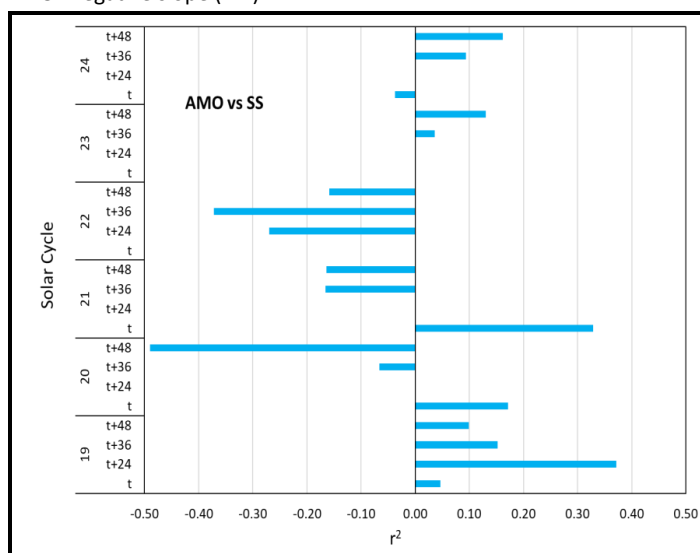


807 **Fig. 5.** Linear regression correlation coefficient r^2 ($p < 0.05$) of SS monthly counts cycles 19-24 against
 808 indexes: ONI (red) and PDO (blue). Negative slope ($-r^2$).



809
 810

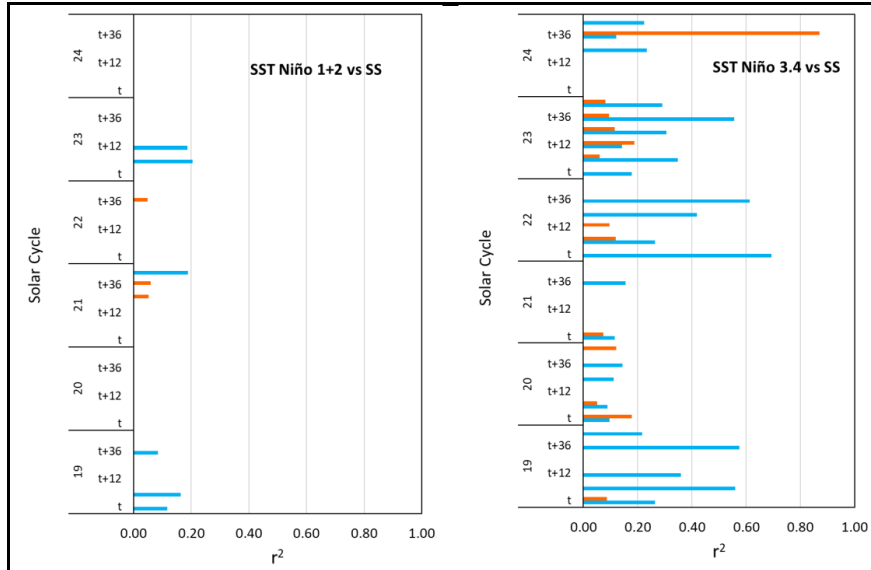
811 **Fig. 6.** Linear regression correlation coefficient r^2 ($p < 0.05$) of SS monthly counts for cycles 19-24
 812 against index AMO. Negative slope ($-r^2$).



813

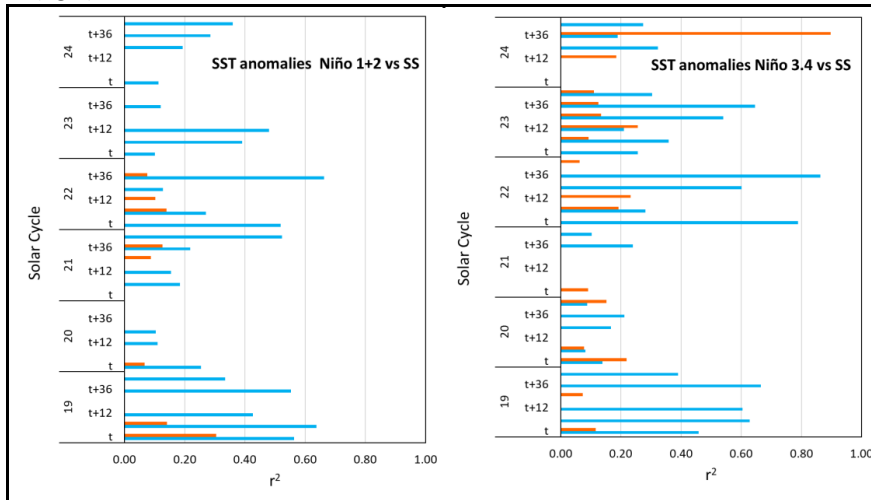


814 **Fig. 7.** Linear regression correlation coefficient r^2 ($p < 0.05$) of SS monthly counts during the ascending
 815 (blue) and descending (red) phases of SS for cycles 19-24 against SST in regions El Niño 1+2 (left) and
 816 3.4 (right).



817
 818

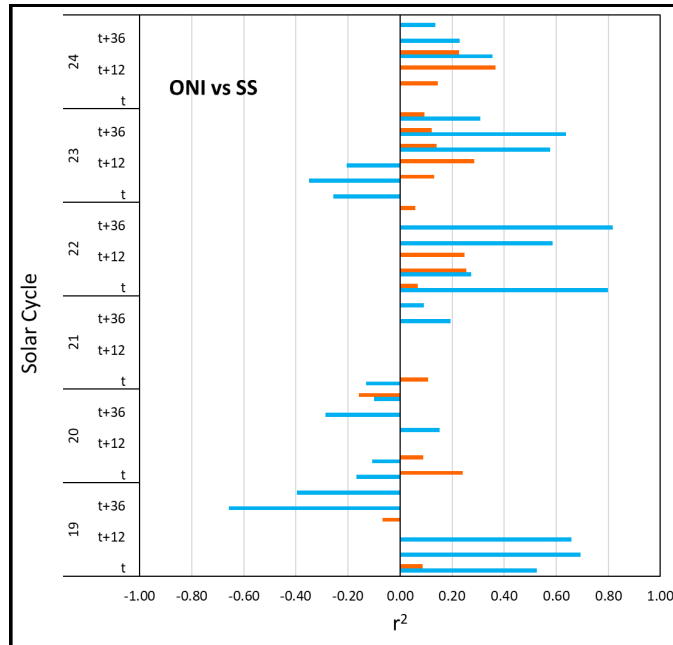
819 **Fig. 8.** Linear regression correlation coefficient r^2 ($p < 0.05$) of SS monthly counts during the ascending
 820 (blue) and declining (red) phases for SS cycles 19-24 against SST Anomaly in regions El Niño 1+2 (left)
 821 and 3.4 (right).



822
 823



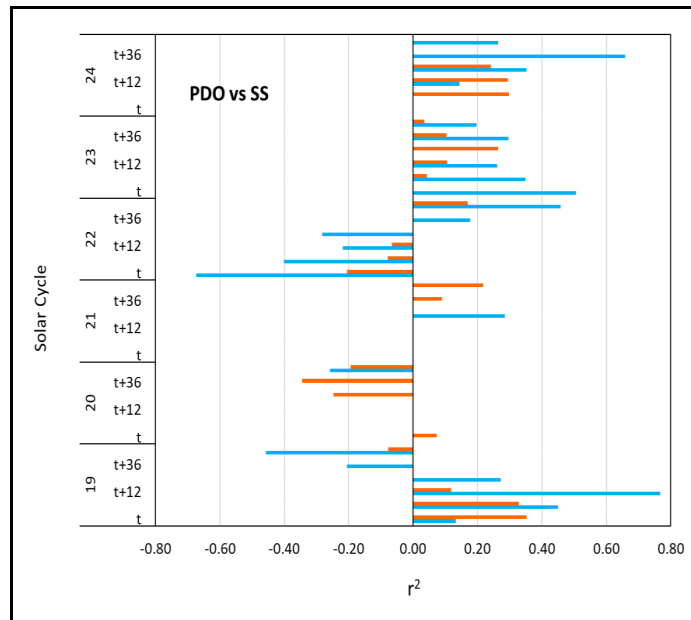
824 **Fig. 9.** Linear regression correlation coefficient r^2 of SS monthly counts during the ascending (blue)
 825 and declining (red) phases of SS cycles (19-24) against index ONI. Negative slope ($-r^2$).



826

827

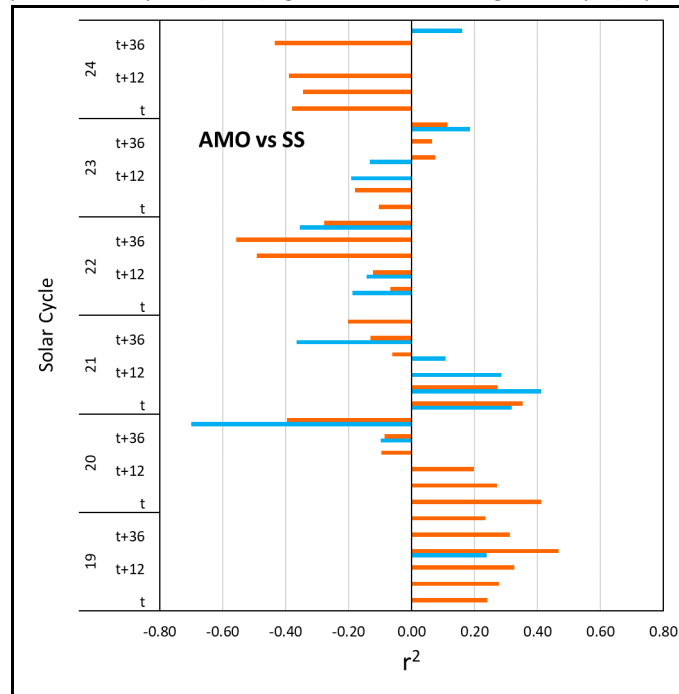
828 **Fig. 10.** Linear regression correlation coefficient r^2 ($p < 0.05$) of SS monthly counts during the
 829 ascending (blue) and declining (red) phases of SS cycles (19-24) against index PDO. Negative slope ($-$
 830 r^2).



831

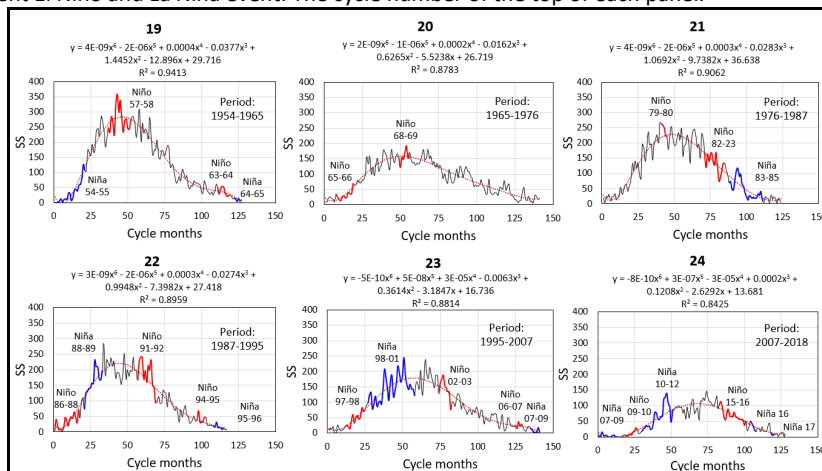


832
 833 **Fig. 11.** Linear regression correlation coefficient r^2 of SS numbers during the ascending (blue) and
 834 declining (red) phases of SS cycles (19-24) against index AMO. Negative slope ($-r^2$)



835
 836

837 **Fig. 12.** Polynomial functions of 6 degrees ($p < 0.001$), based on monthly SS counts. Red and blue lines
 838 represent El Niño and La Niña event. The cycle number of the top of each panel.



839